Selective Binding by the RNA Binding Domain of PKR Revealed by Affinity Cleavage†

Richard J. Spanggord and Peter A. Beal*

Department of Chemistry, University of Utah, Salt Lake City, Utah 84112

Received October 31, 2000; Revised Manuscript Received January 31, 2001

ABSTRACT: The RNA-dependent protein kinase (PKR) is regulated by the binding of double-stranded RNA (dsRNA) or single-stranded RNAs with extensive duplex secondary structure. PKR has an RNA binding domain (RBD) composed of two copies of the dsRNA binding motif (dsRBM). The dsRBM is an α−*β*−*β*−*β*−α structure present in a number of proteins that bind RNA, and the selectivity demonstrated by these proteins is currently not well understood. We have used affinity cleavage to study the binding of PKR's RBD to RNA. In this study, we site-specifically modified the first dsRBM of PKR's RBD at two different amino acid positions with the hydroxyl radical generator EDTA·Fe. Cleavage by these proteins of a synthetic stem−loop ligand of PKR indicates that PKR's dsRBMI binds the RNA in a preferred orientation, placing the loop between strands *β*1 and *β*2 near the single-stranded RNA loop. Additional cleavage experiments demonstrated that defects in the RNA stem, such as an A bulge and two GA mismatches, do not dictate dsRBMI's binding orientation preference. Cleavage of VA_I RNA, an adenoviral RNA inhibitor of PKR, indicates that dsRBMI is bound near the loop of the apical stem of this RNA in the same orientation as observed with the synthetic stem−loop RNA ligands. This work, along with an NMR study of the binding of a dsRBM derived from the *Drosophila* protein Staufen, indicates that dsRBMs can bind stem−loop RNAs in distinct ways. In addition, the successful application of the affinity cleavage technique to localizing dsRBMI of PKR on stem−loop RNAs and defining its orientation suggests this approach could be applied to dsRBMs found in other proteins.

The RNA-dependent protein kinase (PKR)[1] is 68 kDa in size with an approximately 20 kDa N-terminal RNA binding domain and a C-terminal protein kinase domain (*1*). In vitro, PKR is activated by binding to RNA molecules with extensive duplex secondary structure (*2*). In vivo, the enzyme is believed to be activated by viral double-stranded RNA (dsRNA) or viral replicative intermediates comprising dsRNA (*3*). Activated PKR can phosphorylate several protein substrates, including the α-subunit of heterotrimeric eukaryotic translation initiation factor 2 (eIF2α) (*4*). Phosphorylation of eIF2α has the effect of inhibiting continued initiation of protein synthesis by the eIF2 complex (*5*). Viruses that infect eukaryotic cells have evolved mechanisms by which they circumvent the activity of this antiviral kinase. Some, such as adenovirus and Epstein Barr virus, synthesize highly structured RNAs that bind PKR and block activation (VA and EBER RNAs, respectively) (*6*, *7*).

The RNA binding domain of PKR is composed of two copies of the dsRNA binding motif (dsRBM I and dsRBM II), a sequence motif found in many proteins that bind double-stranded RNAs (dsRNA) or single-stranded RNAs with extensive duplex secondary structure (*8*). These proteins are involved in a myriad of biological processes such as RNA editing (*9*), RNA trafficking (*10*), RNA processing (*11*), transcriptional regulation (*12*), and the interferon antiviral response (*13*). Many of these proteins have been shown to bind RNA duplexes without a strict sequence requirement. However, the action of proteins that have dsRBMs in their structure can be quite selective. For instance, PKR has been shown to bind selectively to a site on the hepatitis delta virus genomic RNA (*3*). In addition, the RNA editing adenosine deaminases ADAR1 and ADAR2 efficiently deaminate only a select few adenosines in natural editing substrates (*14*). Other dsRBM proteins have demonstrated selectivity for certain RNA substrates (*15*, *16*). How the binding selectivity of a given dsRBM contributes to the functional selectivity of the protein containing it is an important question for members of this family of RNA binding proteins.

The solution structure of the 20 kDa RNA binding domain of PKR has been determined by NMR spectroscopy (*17*). Each dsRBM consists of an α−*β*−*β*−*β*−α structure where the two α-helices are packed onto one side of a three-stranded

† This work was supported by a grant from the National Institutes of Health to P.A.B. (Grant GM-57214).

* To whom correspondence should be addressed. Telephone: (801) 585-9719. Fax: (801) 581-8433. E-mail: beal@chemistry.chem.utah.

[1] Abbreviations: PKR, RNA-dependent protein kinase; eIF2α, α-subunit of eukaryotic initiation factor 2; RBD, RNA binding domain; bp, base pair; nt, nucleotide; dsRBM, double-stranded RNA binding motif; SDS, sodium dodecyl sulfate; EDTA, ethylenediaminetetraacetic acid; Tris, tris(hydroxymethyl)aminomethane; DTT, dithiothreitol; E29C-EDTA·Fe, GSEE (human PKR residues 1−184) bearing the E29C, C121V, and C135V mutations modified with bromoacetamidobenzyl-EDTA·Fe at position 29; D38C-EDTA·Fe, GSEE (human PKR residues 1−184) bearing the D38C, C121V, and C135V mutations modified with bromoacetamidobenzyl-EDTA·Fe at position 38; VA_I RNA, adenoviral PKR inhibiting RNA I; DMSO, dimethyl sulfoxide; TBE, 90 mM Tris, 90 mM boric acid, and 2 mM EDTA; SELEX, systematic evolution of ligands by exponential enrichment; PMSF, phenylmethanesulfonyl fluoride; THF, tetrahydrofuran; BSA, bovine serum albumin.

10.1021/bi002512w CCC: $20.00
Published on Web 03/14/2001

β-sheet. The two dsRBMs of PKR are separated by a 22-residue linker of poorly defined structure. Although there have been no reports of high-resolution structural data on a PKR−RNA complex, structures of protein−RNA complexes involving motifs from two other members of the dsRBM family have been reported (*18*, *19*). In the crystal structure of dsRBMII from the *Xenopus laevis* protein Xlrbpa bound to duplex RNA, the protein contacts 16 bp of dsRNA along one face of the helix, crossing the major groove and contacting two adjacent minor grooves (*18*). Interestingly, the protein binding site in this structure is composed of nucleotides from two 10 bp duplexes stacked end to end with the dsRBM straddling a major groove that deviates from perfect A-form geometry at the junction. Specificity for RNA over DNA for the dsRBM is explained by the numerous contacts between the protein and the 2′-OH groups in the minor groove in this structure (*20*). The few contacts between the protein and RNA bases also explained the lack of a rigid requirement of a specific sequence of duplex RNA in the binding of dsRBM proteins (*8*). In the NMR structure of dsRBMIII from the *Drosophila* protein Staufen bound to a stem−loop RNA, the single-stranded RNA loop is bound by the N-terminal α-helix (α1) of the dsRBM (*19*). This result indicated that the dsRBM is a more versatile RNA binding module than previously recognized as it can simultaneously bind to both duplex and single-stranded RNA. Indeed, it was suggested that interactions between dsRBM α1 and single-stranded loop sequences may be a general mechanism by which specificity arises in the binding of dsRBM proteins to stem−loop RNAs (*19*). Nagel and Ares recently proposed that the specificity of the yeast RNaseIII homologue Rnt1p for certain stem−loop substrates may arise from the interaction of the AGNN loop sequence with amino acid residues found between strands β1 and β2 of the Rnt1p's dsRBM (*15*). This model invokes a binding orientation on the stem−loop RNA substrate which is the opposite of that found in the Staufen−RNA NMR structure. Thus, even with two high-resolution structures of dsRBMs bound to RNA available, the orientation of a given dsRBM on a stem−loop RNA and, therefore, the amino acids in proximity to the single-stranded loop, cannot be predicted and must be defined experimentally.

In our ongoing work related to understanding the RNA regulation of PKR, we prepared site-specifically modified proteins consisting of PKR's 20 kDa RNA binding domain (RBD) (*21*). These modified proteins have functional groups introduced at different positions to help define features of PKR−RNA complexes. Here we show that PKR RBD proteins modified with EDTA·Fe at two different positions cleave RNA ligands selectively. The cleavage patterns that are generated reveal features of the PKR−RNA complexes. For instance, cleavage of a synthetic stem−loop ligand of PKR indicates that PKR binds this RNA with a preferred orientation, placing the loop between β1 and β2 of dsRBMI near the single-stranded RNA loop (*22*). This binding mode is different from that observed for Staufen dsRBMIII bound to a stem−loop structure and similar to that proposed for the binding of Rnt1p to stem−loop substrates. Removal of the A bulge and two GA mismatches found in this RNA, creating a perfectly matched duplex stem, does not alter the binding preference, suggesting that this preference originates from either the single-stranded loop or the sequence of the duplex itself. Cleavage of the adenovirus VA_I RNA with the EDTA·Fe-modified proteins indicates that dsRBMI binds near the loop of the apical stem of the RNA in the same orientation as with the synthetic stem−loop RNAs. Together, these results indicate that proteins from the dsRBM family can selectively bind stem−loop RNAs in distinct ways. Furthermore, the successful application of the affinity cleavage technique to localizing dsRBMI of PKR on stem−loop RNAs and defining its orientation suggests this approach could be used to study the binding selectivity of other dsRBM proteins.

MATERIALS AND METHODS

General. Distilled, deionized water was used for all aqueous reactions and dilutions. Biochemical reagents were obtained from Sigma/Aldrich unless otherwise noted. Restriction enzymes and nucleic acid-modifying enzymes were purchased from Pharmacia, Boehringer-Mannheim, or New England Biolabs. Oligonucleotides were prepared on a Perkin-Elmer/ABI model 392 DNA/RNA synthesizer with β-cyanoethyl phosphoramidites. 5′-Dimethoxytrityl-protected 2′-deoxyadenosine, 2′-deoxyguanosine, 2′-deoxycytidine, and thymidine phosphoramidites were purchased from Perkin-Elmer/ABI. 5′-Dimethoxytrityl-2′-*tert*-butyldimethylsilyl-protected adenosine, guanosine, cytidine, and uridine phosphoramidites were purchased from Glen Research. [γ-^{32}P]ATP (6000 Ci/mmol) was obtained from DuPont NEN. Storage phosphor autoradiography was carried out using imaging plates purchased from Kodak. A Molecular Dynamics STORM 840 instrument was used to obtain all data from phosphor imaging plates. Bromoacetamidobenzyl-EDTA·Fe was kindly provided by C. Meares at the University of California, Davis (Davis, CA). All NMR and crystal structures were visualized on a Silicon Graphics O_2 workstation running Insight II (Biosym).

Construction of the PKR RBD Single-Cysteine Mutants. As described previously (*21*), mutants of the PKR RBD (amino acids 1−184) were obtained as glutathione *S*-transferase (GST) fusion proteins by expression in *Escherichia coli* using the bacterial expression plasmid pGEX-2T (Pharmacia). An expression plasmid for the cysteine-free PKR RBD was constructed as previously described (*21*). PCR mutagenesis was used to introduce single-cysteine mutations into the cysteine-free PKR RBD expression plasmid. The following primers were used: E29C (mutagenic oligo), 5′-TCCTGAATTAGGCAGACATTGATATTTAA-GTAC-3′; D38C (5′ mutagenic oligo), 5′-CCTAATTCag-gacctCCACATTGTAGGAGGTTT-3′; and PKR RBD template primers, 5′-GCGTGAggatccGAAGAAATGGCTGGT-GATCTT-3′ (5′ primer) and 5′-TCACGCGGTACCTTAA-GTAGCAAAAGAACCAGAGGA-3′ (3′ primer). Lowercase nucleotides represent incorporated restriction sites (D38C *Ppu*MI and PKR RBD template 5′ primer *Bam*HI), and underlined nucleotides represent introduced cysteine mutations. All single-cysteine mutations were verified by DNA sequencing.

Expression and Purification of PKR RBD Proteins. PKR RBD expression and purification were performed as previously described (*21*). Briefly, the BL-21 *E. coli*-expressed GST fusion PKR RBD was incubated with glutathione-Sepharose for 3 h at 4 °C. Unbound proteins were removed

by successive washes with glutathione-Sepharose buffer [20 mM Tris-HCl (pH 8.3), 1 mM DTT, and 1 mM PMSF] and thrombin buffer [120 mM Tris-HCl (pH 8.6), 150 mM NaCl, and 7 mM $CaCl_2$]. The GST domain was removed by incubating the fusion protein with 60 units of thrombin for 12 h at 4 °C, and the reaction was quenched with the addition of PMSF (1 mM final concentration).

Preparation of RNA Ligands of PKR. Generation of the synthetic stem−loop ligands of PKR was performed on a Perkin-Elmer DNA/RNA synthesizer. Deprotection of the synthetic oligoribonucleotides was carried out in NH_3-saturated methanol for 24 h at room temperature followed by 1 M tetrabutylammonium fluoride in THF for 36 h at room temperature. Deprotected oligonucleotides were desalted on a NAP-25 column and purified by denaturing polyacrylamide gel electrophoresis. Purified RNA was visualized by UV shadowing, and extracted from the gel by crushing and soaking in 0.5 M NH_4OAc, 0.1% SDS, and 0.1 mM EDTA overnight. The oligonucleotides were ethanol precipitated, and concentrations were estimated by UV absorbance at 260 nm. End-labeled stem−loop RNAs (5′-^{32}P) were prepared by incubating 10−20 pmol of RNA with [γ-^{32}P]ATP (6000 Ci/mmol, DuPont) and T4 polynucleotide kinase for 1.5 h at 37 °C. Labeled RNA was purified on a 16% polyacrylamide gel and extracted as described above. Labeled stem−loop RNAs (3′-^{32}P) were prepared by treating 20−30 pmol of RNA with [^{32}P]pCp (DuPont) and RNA ligase for 3 h at 37 °C and purified on a 16% denaturing polyacrylamide gel. Labeled RNA was isolated as described above.

VA_I RNA was generated by transcription with T7 RNA polymerase. Generation of the necessary transcription template was performed as a three-piece ligation into the pAlter-1 plasmid (Promega). The DNA template consisted of four synthesized oligos (75mer and 77mer complement/82mer and 80mer complement). The sequences of these oligos are as follows: 75mer oligo, 5′-**aattTCCGTGGTCTGGTGGATAAATTCGCAAGGGTATCATGGCGGACGACCGGGGTTCGAACCCCGGATCCGGCC-3′**; its complementary 77mer oligo, 5′-GCGGACGGCCGGATCCGGGGTTCGAACCCCGGTCGTCCGCCATGATACCC-TTGCGAATTTATCCACCAGACCACGGA-3′; 82mer oligo, 5′-**GTCCGCCGTGATCCATGCGGTTACCGCCCGCGTGTCGAACCCAGGTGTGCGACGTCAGACAACGGGGATGCGCTCCTTT**AAA-3′; and its complementary 80mer oligo, 5′-agctTTTAAAGGAGCGCATCCCCGTTGTCTGACGTCGCACACCTGGGTTCGACACGCGGGCGGTAACCGCATGGATCACG-3′. Bold nucleotides represent the VA_I RNA sequence (*23*) (represented in the 75mer and 82mer oligos), and underlined nucleotides represent the complementary ends that will anneal to form a duplex insert containing the transcription template. Lowercase nucleotides represent the incorporated restriction sites that allow the ligation of the duplex insert into the *Eco*RI- and *Hin*dIII-digested pAlter-1 plasmid (*Eco*RI overhang in the 75mer and *Hin*dIII overhang in the 80mer). The VA_I RNA−DNA template was verified by DNA sequencing. T7 RNA polymerase was used to generate the 159 nt VA_I RNA. Transcription mixtures were heated to 70 °C for 10 min and then purified on a 12% denaturing polyacrylamide gel. Bands were visualized via UV shadowing and excised from the gel by the crush and soak method described above. Labeled RNA (5′-^{32}P) was prepared by treating 100 pmol of transcript with shrimp alkaline phosphatase (SAP) for 2 h at 37 °C followed by phenol/chloroform extraction and ethanol precipitation. The SAP-treated transcript was purified and isolated as described above. Dephosphorylated RNA was labeled using polynucleotide kinase and [γ-^{32}P]ATP and purified on a 12% denaturing polyacrylamide gel. Labeled RNA was isolated as described above. Labeling (3′-^{32}P) of VA_I RNA was performed as described above except dephosphorylated RNA was used and purified on a 12% denaturing polyacrylamide gel.

Bromoacetamidobenzyl-EDTA·Fe Modification of Single-Cysteine PKR RBD Mutants. Conjugation of the PKR RBD cysteine mutants with the nucleic acid cleaving reagent bromoacetamidobenzyl-EDTA·Fe was performed initially by incubating 300 μL of a 100−250 μM PKR RBD solution with 1 mM DTT for 12 h at 4 °C. The solution was dialyzed into degassed modification buffer [10 mM Hepes (pH 8.0), 0.1 M NaCl, 5% glycerol, and 0.1 mM EDTA] until all the DTT had been removed (3 h). The PKR RBD (250 μL solution) was mixed with 11.5 μL of a 26 mM solution of bromoacetamidobenzyl-EDTA·Fe (in DMSO) followed by a 3 h incubation at 37 °C. Conjugation reactions were quenched by the removal of excess reagent with immediate dialysis into storage buffer [25 mM Tris-HCl (pH 7.0) and 10 mM NaCl] in the dark at 4 °C. The derivatized PKR RBD concentration was determined by Bio-Rad protein assays with BSA as a protein standard. Bromoacetamidobenzyl-EDTA·Fe-modified proteins were stored at −20 °C. The extent of conjugation was analyzed via electrospray ionization mass spectrometry as previously described (*21*). The calculated molecular mass for PKR RBD (E29C/C121V/C135V)-EDTA·Fe was 21 120 Da (found, 21 119 Da). The calculated molecular mass for PKR RBD (D38C/C121V/C135V)-EDTA·Fe was 21 134 Da (found, 21 132 Da).

Affinity Cleavage Experiments. RNA complexes with PKR RBD-EDTA·Fe conjugates were formed by incubating the protein with 5′- and 3′-end-labeled RNA at room temperature for 7 min in 25 mM Tris-HCl (pH 7.0) and 10 mM NaCl. Protein−RNA complexes were analyzed via gel mobility shift assays as previously described (*21*). PKR RBD−RNA complexes (20 μL final reaction volume) were probed by initiating hydroxyl radical formation with 0.01% hydrogen peroxide and 5 mM sodium ascorbate followed by incubation at room temperature for 1 min. Reactions were quenched by the addition of 80 μL of distilled water followed by phenol/chloroform extraction and ethanol precipitation. Cleaved RNA was resuspended into 10 μL of formamide loading dye and analyzed via denaturing polyacrylamide gel electrophoresis. Data were obtained from the gels using storage phosphor autoradiography and a STORM phosphorimager (Molecular Dynamics). Mapping of the cleavage data was performed using Image Quant software (Molecular Dynamics). Traces were generated for gel lanes corresponding to RNA with unmodified or modified protein added in the presence of hydrogen peroxide and sodium ascorbate. Intensities of the cleavage bands were measured and mapped onto the secondary structures of each RNA that was studied.

RESULTS

Cleavage of Synthetic Stem−Loop Ligands of PKR with Two Different RBD-EDTA·Fe Proteins. To define structural

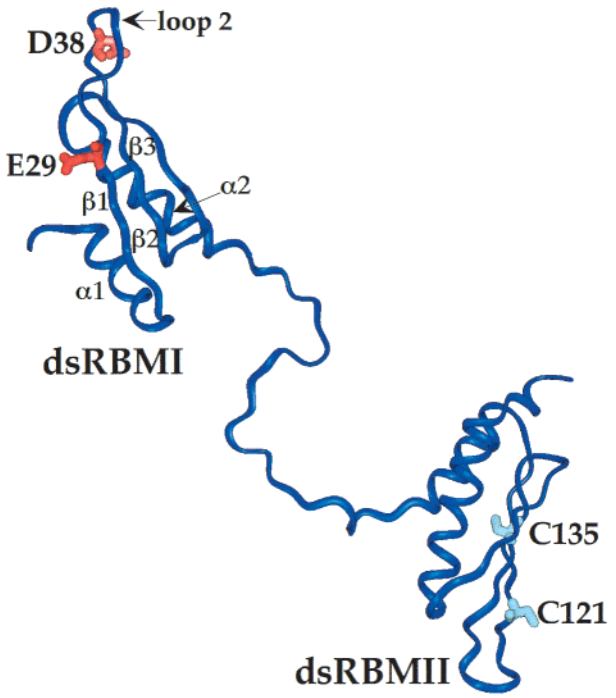

FIGURE 1: Structure of the PKR RBD (amino acids 11−179) showing the locations of amino acids selected for mutagenesis in dsRBMI (red) along with the two natural cysteines in dsRBMII (blue) (*17*).

features of PKR RBD−RNA complexes, we employed the affinity cleavage technique. This approach involves the covalent attachment of a nonselective cleavage reagent to specific positions in the nucleic acid binding molecule and analysis of the cleavage patterns generated by these conjugates (*24*). This method was used to analyze the binding of PKR's RNA binding domain, which is located in the first 184 amino acids of the protein (*25*). This domain can be expressed independently to high levels in bacteria and easily purified. Earlier, we demonstrated that two cysteine residues found naturally in PKR's RBD are not essential for RNA-regulated kinase activity (*21*). Furthermore, several single-cysteine mutants of PKR's RBD could be modified with cysteine-specific reagents without significant loss of RNA binding activity. To generate proteins for affinity cleavage experiments, we overexpressed two single-cysteine mutants of PKR's RBD (E29C/C121V/C135V) and (D38C/C121V/C135V). The E29C mutation is located near the center of dsRBMI along strand β1 (Figure 1). D38C is closer to one end of dsRBMI in loop 2 between strands β1 and β2 (Figure 1). The two mutants were modified with the cysteine selective bromoacetamidobenzyl-EDTA·Fe, introducing the hydroxyl radical generator EDTA·Fe at either amino acid position 29 or 38 (*26*). Electrospray ionization mass spectrometry was used to confirm stoichiometric modification for both proteins (*21*). Gel mobility shift experiments with several RNAs showed the two modified proteins had similar binding affinities (data not shown).

For our initial studies, we chose to analyze the cleavage patterns generated on a stem−loop RNA identified as the minimal variant of a PKR ligand discovered in a SELEX experiment (*22*). This 46 nt synthetic stem−loop RNA was prepared by automated RNA synthesis and end labeled with

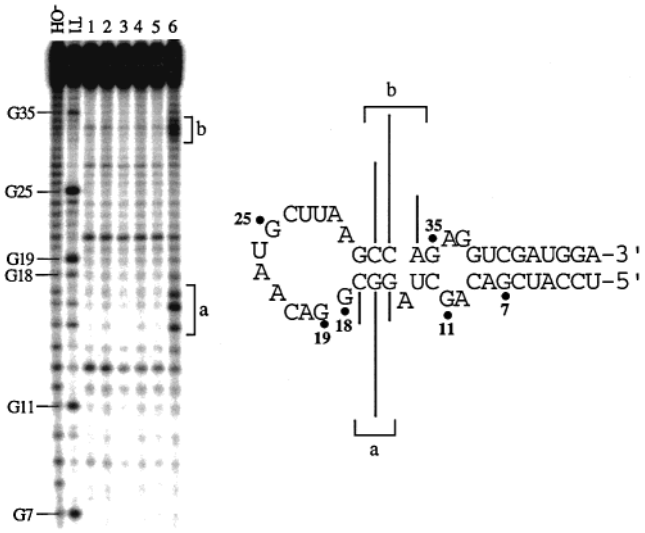

FIGURE 2: Affinity cleaving of a synthetic stem−loop ligand of PKR using the EDTA·Fe-modified E29C PKR RBD mutant. Shown at the left is a storage phosphor autoradiogram of a 16% denaturing polyacrylamide gel separating the 5′-end-labeled RNA cleavage products. Major cleavage sites are identified with letters and brackets. This RNA was 3′-end-labeled to investigate the 3′ end of the RNA for any additional cleavage sites. No other major cleavage sites were observed: −OH, alkaline hydrolysis; T1, T1 RNase; lane 1, RNA with no added hydrogen peroxide or sodium ascorbate; lane 2, RNA in the presence of 0.01% hydrogen peroxide and 5 mM sodium ascorbate; lane 3, 6 μM unmodified E29C PKR RBD and RNA with no added hydrogen peroxide or sodium ascorbate; lane 4, 6 μM unmodified E29C PKR RBD and RNA in the presence of 0.01% hydrogen peroxide and 5 mM sodium ascorbate; lane 5, 6 μM EDTA·Fe-modified E29C PKR RBD and RNA with no added hydrogen peroxide or sodium ascorbate; and lane 6, 6 μM EDTA·Fe-modified E29C PKR RBD and RNA in the presence of 0.01% hydrogen peroxide and 5 mM sodium ascorbate. Shown at the right is the mapping of the major cleavage sites (identified by letters and brackets) on the stem−loop RNA's predicted secondary structure. The secondary structure has been confirmed by mutagenesis experiments (*22*). Lines indicate sites of cleavage, and line lengths indicate relative cleavage efficiencies.

^{32}P for the analysis (Figures 2 and 3). Importantly, the E29C-EDTA·Fe conjugate cleaved the RNA selectively at the end of the duplex near the single-stranded loop (Figure 2). The cleavage was observed only with the EDTA·Fe-modified protein and was dependent on the addition of hydrogen peroxide and sodium ascorbate (Figure 2, lanes 1−6). Thus, this cleavage arises from hydroxyl radicals generated from the covalently attached EDTA·Fe, indicating that amino acid position 29 is in proximity (approximately <25 Å) to base pairs located near the RNA loop (*27*). The observed cleavage was selective with no other sites found on this RNA either 5′ or 3′ end-labeled (latter not shown). When the D38C-EDTA·Fe conjugate was used to cleave this RNA, again selective cleavage was observed (Figure 3). A higher level of background cleavage was observed with this protein, likely due to the placement of the EDTA·Fe in flexible loop 2 between β1 and β2. However, with this protein, nucleotides in the loop near the base-paired stem were cleaved most efficiently (Figure 3). Therefore, the amino acid at position 38 is proximal to the RNA loop in the protein−RNA complex. The relative locations of the two cleavage patterns generated by the two EDTA·Fe-modified proteins indicate that dsRBMI of PKR binds this synthetic stem−loop motif

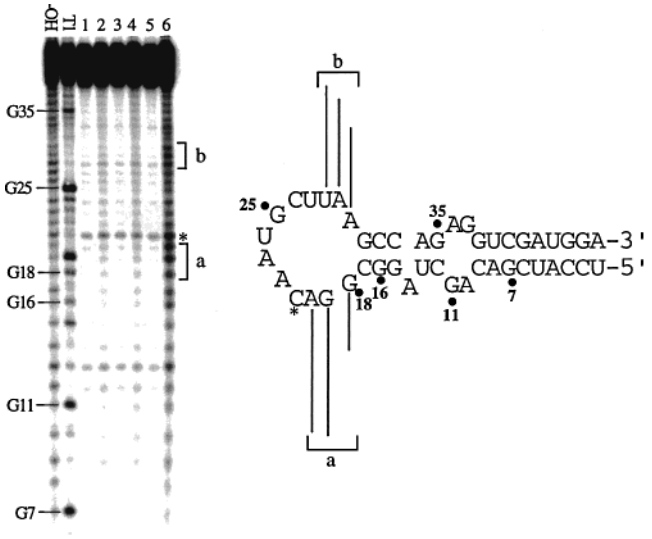

FIGURE 3: Affinity cleaving of the synthetic stem−loop ligand of PKR using the EDTA·Fe-modified D38C PKR RBD mutant. Shown at the left is a storage phosphor autoradiogram of a 16% denaturing polyacrylamide gel separating the 5′-end-labeled RNA cleavage products. Major cleavage sites are identified with letters and brackets. This RNA was 3′-end-labeled to investigate the 3′ end of the RNA for any additional cleavage sites. No other major cleavage sites were observed: −OH, alkaline hydrolysis; T1, T1 RNase; lane 1, RNA with no added hydrogen peroxide or sodium ascorbate; lane 2, RNA in the presence of 0.01% hydrogen peroxide and 5 mM sodium ascorbate; lane 3, 6 μM unmodified D38C PKR RBD and RNA with no added hydrogen peroxide or sodium ascorbate; lane 4, 6 μM unmodified D38C PKR RBD and RNA in the presence of 0.01% hydrogen peroxide and 5 mM sodium ascorbate; lane 5, 6 μM EDTA·Fe-modified D38C PKR RBD and RNA with no added hydrogen peroxide or sodium ascorbate; and lane 6, 6 μM EDTA·Fe-modified D38C PKR RBD and RNA in the presence of 0.01% hydrogen peroxide and 5 mM sodium ascorbate. Shown at the right is the mapping of the major cleavage sites (identified by letters and brackets) on the minimal binding RNA ligand's secondary structure (*22*). C21, denoted with an asterisk, is cleaved in the absence of the EDTA·Fe-modified protein and is not included in the mapping of EDTA·Fe−PKR RBD specific cleavage sites.

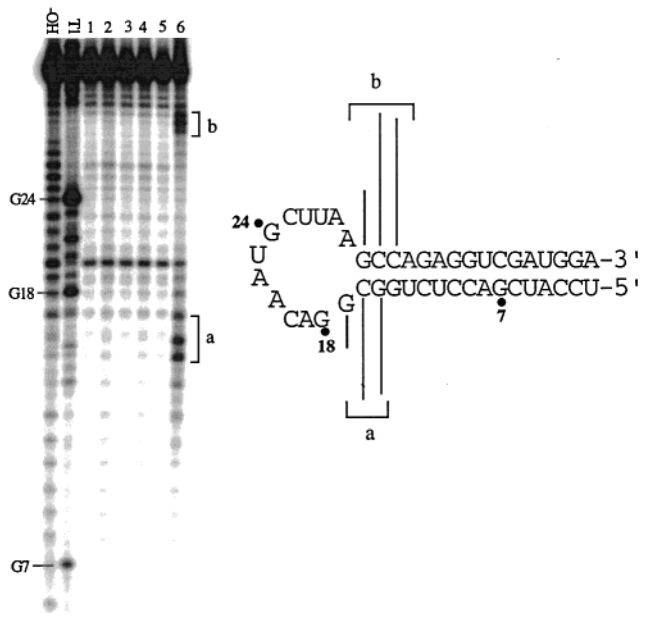

FIGURE 4: Affinity cleaving of the mutant stem−loop ligand of PKR using the EDTA·Fe-modified E29C PKR RBD mutant. Shown at the left is a storage phosphor autoradiogram of a 16% denaturing polyacrylamide gel separating the 5′-end-labeled RNA cleavage products. Major cleavage sites are identified with letters and brackets. This RNA was 3′-end-labeled to investigate the 3′ end of the RNA for any additional cleavage sites. No other major cleavage sites were observed: −OH, alkaline hydrolysis; T1, T1 RNase; lane 1, RNA with no added hydrogen peroxide or sodium ascorbate; lane 2, RNA in the presence of 0.01% hydrogen peroxide and 5 mM sodium ascorbate; lane 3, 6 μM unmodified E29C PKR RBD and RNA with no added hydrogen peroxide or sodium ascorbate; lane 4, 6 μM unmodified E29C PKR RBD and RNA in the presence of 0.01% hydrogen peroxide and 5 mM sodium ascorbate; lane 5, 6 μM EDTA·Fe-modified E29C PKR RBD and RNA with no added hydrogen peroxide or sodium ascorbate; and lane 6, 6 μM EDTA·Fe-modified E29C PKR RBD and RNA in the presence of 0.01% hydrogen peroxide and 5 mM sodium ascorbate. Shown at the right is the mapping of the major cleavage sites (identified by letters and brackets) on the mutant stem loop ligand's secondary structure.

in a specific orientation placing loop 2 between β1 and β2 near the RNA loop.

Due to the observed binding preference of the PKR's dsRBMI found with the stem−loop ligand, we examined whether this preference originated from the two GA mismatches and A bulge. A mutant RNA was constructed consisting of the stem−loop region where the two GA mismatches were converted to two Watson−Crick base pairs and the A bulge had been removed, creating a stem−loop sequence containing an uninterrupted 16 bp duplex (Figures 4 and 5). The predicted secondary structure of this RNA is consistent with the relatively low reactivity of the nucleotides in the duplex stem under the conditions of both alkaline hydrolysis and T1 nuclease digestion compared to the reactivity of nucleotides in the single-stranded loop (Figures 4 and 5, lanes −OH and T1). Again, both the E29C- and D38C-EDTA·Fe conjugates selectively cleaved this RNA (Figures 4 and 5). With the E29C-EDTA·Fe conjugate, cleavage was observed at the base of the loop in the duplexed region as observed with the original stem−loop ligand (compare Figures 2 and 4). Also, with the D38C-EDTA·Fe conjugate, nucleotides in the loop of the RNA were observed to be cleaved most efficiently (compare Figures 3 and 5). Therefore, the PKR RBD binds this RNA at the same site in the same orientation as found with the original stem−loop RNA ligand, indicating that the GA mismatches and the A bulge do not dictate the binding selectivity.

Cleavage of the Adenovirus PKR Inhibitor VA$_I$ RNA. Several naturally occurring RNA ligands of PKR have stem−loop structures located in the PKR binding site (*28*, *29*). To determine if PKR's dsRBMI bound one of these RNAs selectively, we analyzed the cleavage patterns generated by E29C-EDTA·Fe and D38C-EDTA·Fe on VA$_I$ RNA, an inhibitor of PKR's activation generated by adenovirus 2 (Figures 6 and 7) (*6*). The E29C-EDTA·Fe conjugate cleaved VA$_I$ RNA selectively with the most efficiently cleaved nucleotides located in base pairs near the loop end of the apical stem (Figure 6). The location of these cleavage sites was confirmed with 3′-end-labeled RNA. To ensure that these cleavage events were due to the bound EDTA·Fe-modified protein, we compared the cleavage products to those generated by free EDTA·Fe and unmodified protein at the same concentration (Figure 6, lane 5). Although some sites cleaved in the presence of the E29C-EDTA·Fe RBD were found with the free EDTA·Fe (e.g., sites in the central domain and C68 in the apical loop), the major cleavage sites in the stem near the apical loop were only detected with the RBD-EDTA·Fe conjugate. Interestingly, Mathews had previously shown

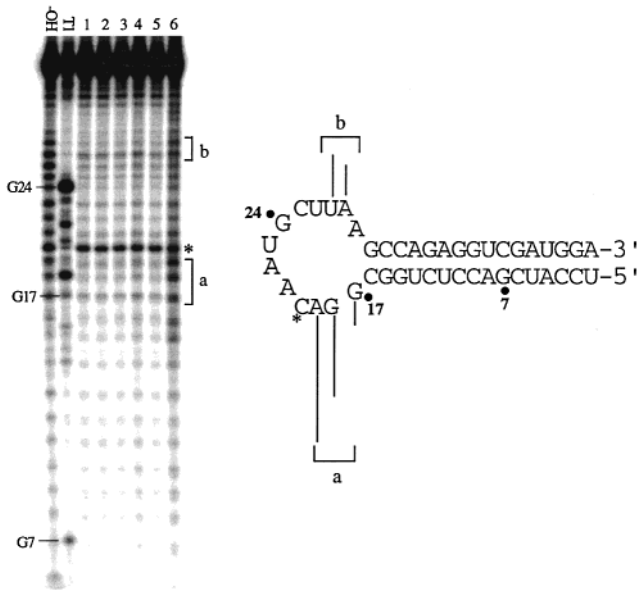

FIGURE 5: Affinity cleaving of the mutant stem−loop ligand of PKR using the EDTA·Fe-modified D38C PKR RBD mutant. Shown at the left is a storage phosphor autoradiogram of a 16% denaturing polyacrylamide gel separating the 5′-end-labeled RNA cleavage products. Major cleavage sites are identified with letters and brackets. This RNA was 3′-end-labeled to investigate the 3′ end of the RNA for any additional cleavage sites. No other major cleavage sites were observed: −OH, alkaline hydrolysis; T1, T1 RNase; lane 1, RNA with no added hydrogen peroxide or sodium ascorbate; lane 2, RNA in the presence of 0.01% hydrogen peroxide and 5 mM sodium ascorbate; lane 3, 6 μM unmodified D38C PKR RBD and RNA with no added hydrogen peroxide or 5 mM sodium ascorbate; lane 4, 6 μM unmodified D38C PKR RBD and RNA in the presence of 0.01% hydrogen peroxide and 5 mM sodium ascorbate; lane 5, 6 μM EDTA·Fe-modified D38C PKR RBD and RNA with no added hydrogen peroxide or sodium ascorbate; and lane 6, 6 μM EDTA·Fe-modified D38C PKR RBD and RNA in the presence of 0.01% hydrogen peroxide and 5 mM sodium ascorbate. Shown at the right is the mapping of the major cleavage sites (identified by letters and brackets) on the mutant stem loop ligand's secondary structure. C20, denoted with an asterisk, is cleaved in the absence of the EDTA·Fe-modified protein and is not included in the mapping of EDTA·Fe−PKR RBD specific cleavage sites.

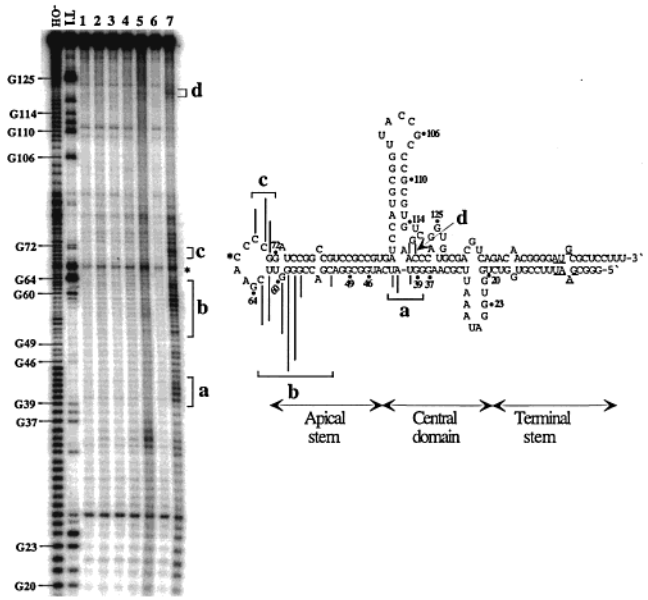

FIGURE 6: Affinity cleaving of the adenovirus VA_I RNA (a PKR kinase inhibitor) using the EDTA·Fe-modified E29C PKR RBD mutant. Shown at the left is a storage phosphor autoradiogram of a 12% denaturing polyacrylamide gel separating the 5′-end-labeled RNA cleavage products. Major cleavage sites are identified with letters and brackets. VA_I RNA was 3′-end-labeled to investigate the 3′ end of the RNA for any additional cleavage sites. No other major cleavage sites were observed: −OH, alkaline hydrolysis; T1, T1 RNase; lane 1, RNA with no added hydrogen peroxide or sodium ascorbate; lane 2, RNA in the presence of 0.01% hydrogen peroxide and 5 mM sodium ascorbate; lane 3, 6 μM unmodified E29C PKR RBD and RNA with no added hydrogen peroxide or sodium ascorbate; lane 4, 6 μM unmodified E29C PKR RBD and RNA in the presence of 0.01% hydrogen peroxide and 5 mM sodium ascorbate; lane 5, 6 μM unmodified E29C PKR RBD and RNA in the presence of 6 μM free EDTA·Fe with 0.01% hydrogen peroxide and 5 mM sodium ascorbate; lane 6, 6 μM EDTA·Fe-modified E29C PKR RBD and RNA with no added hydrogen peroxide or sodium ascorbate; and lane 7, 6 μM EDTA·Fe-modified E29C PKR RBD and RNA in the presence of 0.01% hydrogen peroxide and 5 mM sodium ascorbate. Shown at the right is the mapping of the major cleavage sites (identified by letters and brackets) on the secondary structure model of the adenovirus VA_I RNA. C67, denoted with an asterisk, is cleaved in the absence of the EDTA·Fe-modified protein and is not included in the mapping of EDTA·Fe−PKR RBD specific cleavage sites. Underlined nucleotides represent sequence changes made to facilitate cloning. This region of VA_I RNA is outside the previously described PKR binding site (*29*).

using footprinting techniques that this stem structure was indeed the binding site on VA_I RNA for both the RBD of PKR and the full-length enzyme (*3*, *29*). We also observe weak cleavage in the central domain of VA_I RNA with this conjugate with little cleavage apparent in the terminal stem.

With the D38C-EDTA·Fe protein, the major cleavage pattern was located closer to the loop than observed with the E29C-EDTA·Fe protein. The cleavage occurred at nucleotides that make up the stem−loop junction for the apical stem (Figure 7). With this protein, little cleavage was detected in either the central domain or the terminal stem. Taken together, the results of the cleavage experiments indicate that position 29 of dsRBMI of PKR is located near base pairs at the loop end of the apical stem of VA_I RNA, and position 38, which is in loop 2 of dsRBMI, is located closer to the RNA loop of the apical stem. This orientation of dsRBMI is the same as that observed for the synthetic stem−loop RNAs described above.

DISCUSSION

Affinity cleavage experiments using proteins modified with nonselective nucleic acid cleavage reagents have proven to be useful in defining structural features of a variety of complexes between nucleic acids and proteins (*30*−*32*). Given the fact that dsRBM-containing proteins can typically bind multiple RNAs and the binding site and orientation of a dsRBM on an RNA ligand is often difficult to predict, affinity cleavage experiments have the potential to be valuable in further defining the basis for the observed binding selectivity. However, to our knowledge, this work constitutes the first application of this technique to the study of a member of the dsRBM protein family. Here, we covalently attached EDTA·Fe to different locations in dsRBMI of the RNA binding domain of PKR and used these proteins to study the complexes formed with RNAs containing stem−loop structures. With all of the RNAs studied in this work, highly localized cleavage was observed with the EDTA·Fe conjugates. The results demonstrate that these RNAs have a limited number of binding sites for PKR. Indeed, the

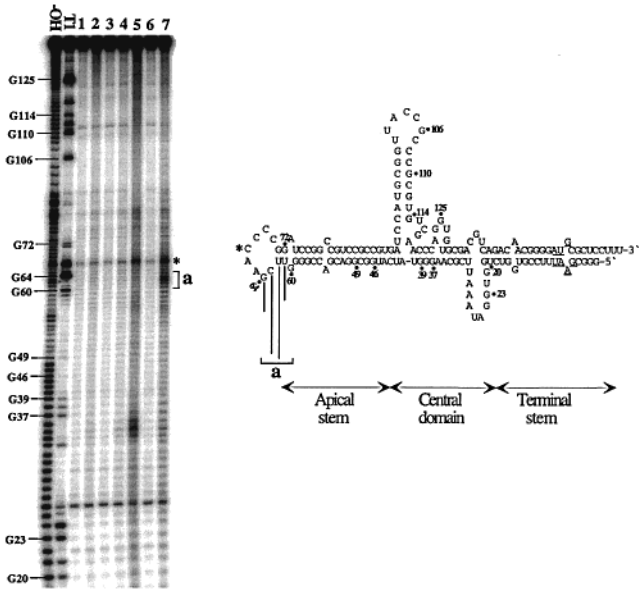

FIGURE 7: Affinity cleaving of the adenovirus VA_I RNA using the EDTA·Fe-modified D38C PKR RBD mutant. Shown at the left is a storage phosphor autoradiogram of a 12% denaturing polyacrylamide gel separating the 5′-end-labeled RNA cleavage products. Major cleavage sites are identified with letters and brackets. VA_I RNA was 3′-end-labeled to investigate the 3′ end of the RNA for any additional cleavage sites. No other major cleavage sites were observed: −OH, alkaline hydrolysis; T1, T1 RNase; lane 1, RNA with no added hydrogen peroxide or sodium ascorbate; lane 2, RNA in the presence of 0.01% hydrogen peroxide and 5 mM sodium ascorbate; lane 3, 6 μM unmodified D38C PKR RBD and RNA with no added hydrogen peroxide or sodium ascorbate; lane 4, 6 μM unmodified D38C PKR RBD and RNA in the presence of 0.01% hydrogen peroxide and 5 mM sodium ascorbate; lane 5, 6 μM unmodified D38C PKR RBD and RNA in the presence of 6 μM free EDTA·Fe with 0.01% hydrogen peroxide and 5 mM sodium ascorbate; lane 6, 6 μM EDTA·Fe-modified D38C PKR RBD and RNA with no added hydrogen peroxide or sodium ascorbate; and lane 7, 6 μM EDTA·Fe-modified D38C PKR RBD and RNA in the presence of 0.01% hydrogen peroxide and 5 mM sodium ascorbate. Shown at the right is the mapping of the major cleavage sites (identified by letters and brackets) on the secondary structure model of the adenovirus VA_I RNA (*29*).

localized cleavage observed with the small stem−loop structures is consistent with a single, high-affinity site for the protein with loop 2 of dsRBMI located near the loop end of the stem. The observed cleavage sites also do not change or increase in number upon addition of larger amounts of protein (data not shown). Furthermore, the location of cleaved nucleotides on VA_I RNA correlates with previous footprinting experiments localizing the PKR binding site to the apical stem (*3*, *29*). Our data show that loop 2 between strands β1 and β2 of dsRBMI from PKR's RBD associates with the loop end of the apical stem of VA_I RNA.

The location of the cleavage patterns we observed on the stem−loop RNA ligands depended on the amino acid position of the PKR RBD modified with EDTA·Fe. For instance, with the E29C-EDTA·Fe conjugate, the 46 nt stem−loop structure was cleaved at the base pairs immediately preceding the single-stranded loop (Figure 2). With the D38C-EDTA·Fe conjugate, the cleavage pattern was shifted on each strand 3−4 nt into the single-stranded loop (Figure 3). This result agrees well with the separation of these amino acid positions found in the Xlrbpa dsRBMII−RNA crystal structure (*18*). In this structure, the accessible nucleotides closest to V133 and K142 (residues in positions analogous to E29 and D38 of PKR) are separated by 3−4 bp. Furthermore, this structure suggests that nucleotides most efficiently cleaved by a dsRBM modified with EDTA·Fe at the amino acid position corresponding to V133 would be within the motif's 16 bp binding site near one end, whereas nucleotides cleaved by a dsRBM modified at the K142 position would likely be outside the 16 bp binding site. Consistent with this prediction, we observe nucleotides in the 4 bp at the loop end of the stem loop cleaved with the E29C-EDTA·Fe conjugate and nucleotides in the adjacent loop cleaved with the D38C-EDTA·Fe conjugate. An important implication of the relative positions of the cleavage patterns observed with the PKR EDTA·Fe conjugates is the orientation of dsRBMI on the stem−loop RNA, placing it with the dsRBMI loop 2 near the single-stranded RNA loop. The cleavage results do not appear to fit a binding orientation with α1 bound in the single-stranded loop, as observed in the Staufen dsRBMIII−RNA NMR structure (*19*). If PKR's dsRBMI were bound in this way, we would expect to see the D38C-EDTA·Fe cleavage pattern shift (relative to the location of the E29C-EDTA·Fe pattern) into the duplex region and not into the single-stranded loop of the RNA. Thus, dsRBMI of PKR binds the stem−loop RNAs studied here in an orientation different from that observed for Staufen's dsRBMIII. This orientation preference could arise from differences in the amino acids found on the RNA binding surface of two dsRBMs or differences in the structures of the stem−loop RNAs that were studied.

The RBD of PKR has been shown to have a minimum binding site on duplex RNA of 16 bp, a result consistent with the amount of RNA contacted in the Xlrbpa dsRBMII−RNA crystal structure (*18*, *20*). If we consider binding modes in which dsRBMI makes contacts only with the duplex of the synthetic stem−loop structures, there are two possible orientations for dsRBMI on these RNAs: with loop 2 near the single-stranded RNA loop or with loop 2 contacting the duplex near the 5′ and 3′ ends of the RNA. The cleavage patterns observed indicate that dsRBMI binds with loop 2 near the single-stranded RNA loop and not in an orientation placing loop 2 near the end of the duplex opposite this loop. If dsRBMI bound in the latter orientation, we would expect to observe nucleotides cleaved with the E29C-EDTA·Fe conjugate in the duplex region proximal to the 5′ and 3′ ends. This result was not observed, and we conclude that dsRBMI of PKR binds selectively in one orientation on the synthetic stem−loop structures.

With the orientation of dsRBMI and the approximate location of loop 2 within the complex defined by our cleavage experiments, we suggest that dsRBMI of PKR binds the stem−loop RNAs as shown in Figure 8. This model was generated by positioning dsRBMI of PKR on the RNA, maintaining the three regions of contact observed in the Xlrbpa dsRBMII−RNA crystal structure (*18*). This places loop 2 and α1 in adjacent minor grooves and the loop between β3 and α2 in the bridging major groove. The model was further refined using our cleavage data, which localize loop 2 near the junction between the duplex and single-stranded RNA loop. This model predicts close proximity between amino acids found in loop 2 of dsRBMI and the single-stranded RNA loop. Interestingly, Nagel and Ares recently proposed that the specificity of Rnt1p for certain

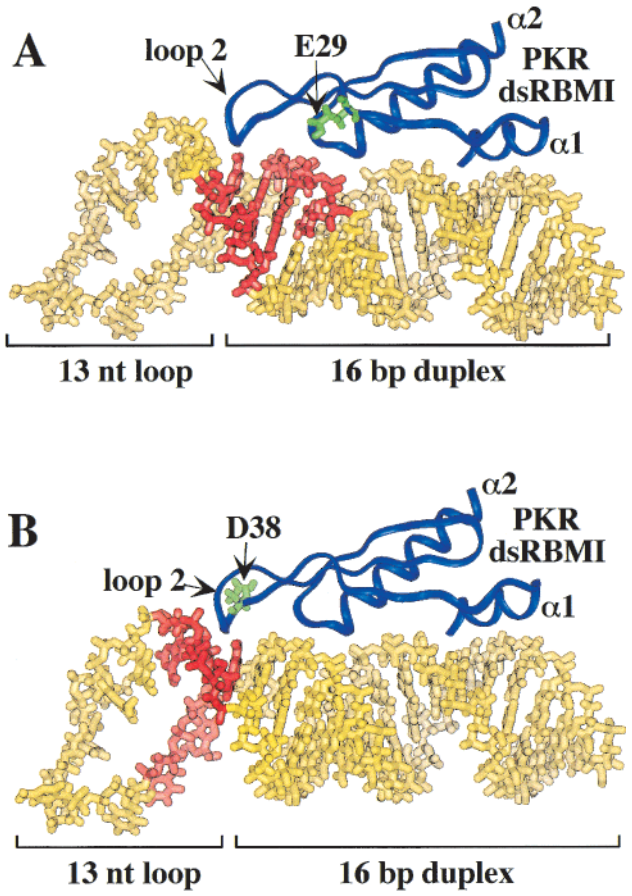

FIGURE 8: Model of the complex formed by the binding of PKR's dsRBMI to the stem−loop RNA described in the legends of Figures 4 and 5. EDTA·Fe-modified amino acid positions are shown in green with the nucleotides cleaved by each modified protein shown in red. (A) Nucleotides cleaved by EDTA·Fe-modified E29C PKR RBD highlighted along with the location of the modified amino acid position in PKR's dsRBMI. (B) Nucleotides cleaved by EDTA·Fe-modified D38C PKR RBD highlighted along with the location of the modified amino acid position in PKR's dsRBMI. A model of the 45 nt stem−loop RNA was generated using InsightII. The PKR dsRBMI shown is a homology model generated using the crystal structure coordinates reported for Xlrbpa's dsRBMII (*18*). Docking was carried out manually in InsightII, maintaining the locations of the three regions of RNA contact observed in the Xlrbpa dsRBMII·RNA structure (*18*) and guided by the cleavage data obtained in this work.

stem−loop substrates may arise from the interaction of RNA loop nucleotides with amino acid residues found in loop 2 of the Rnt1p's dsRBM (*15*). This proposal seems quite plausible in light of the results presented here on the binding of PKR's dsRBMI.

When VA_I RNA was analyzed with the two different EDTA·Fe conjugates, again the major cleavage site observed with D38C-EDTA·Fe was shifted 3−4 nt closer to the single-stranded loop than that of the E29C-EDTA·Fe conjugate (Figures 6 and 7). This result suggests that dsRBMI is oriented on the apical stem of VA_I RNA with loop 2 proximal to the single-stranded RNA loop. This is the same orientation of dsRBMI observed with the synthetic stem−loop RNAs. However, it should be noted that the cleavage patterns generated by the EDTA·Fe conjugates on VA_I RNA are not identical to the patterns present on the synthetic stem−loop RNAs. For instance, one of the strands in the duplex region at the apical stem−loop junction is cleaved more efficiently than the other strand for both conjugates (see Figures 6 and 7). Indeed, efficient cleavage is observed only on one strand in this region for the D38C-EDTA·Fe conjugate. We attribute these subtle differences in cleavage patterns to differences in the structure of the RNAs, leading to differences in accessibility of the adjacent nucleotides.

What is the origin of binding selectivity observed for a protein composed of dsRBMs for which no apparent duplex sequence requirement exists? Several authors have addressed this issue for various members of the dsRBM family of proteins (*3*, *29*, *33*). The deformations (mismatches and bulges) in the stems of RNA ligands can limit the number of binding sites that can be accessed by the protein (*33*). However, we find that removing the bulged nucleotide and replacing the two GA mismatches with Watson−Crick base pairs in the synthetic stem−loop RNA does not affect PKR's binding preference (Figures 4 and 5). The presence of multiple dsRBMs in the RNA binding domain of the protein could lead to a unique structural complementarity between the protein and RNA ligand (*16*). Thus, PKR's dsRBMII may play a role in dictating binding selectivity. It also remains a possibility that specific sequences in the RNA lead to the preferential binding. Indeed, the sequence of the duplex in the stem may produce local deviations from perfect A-form geometry, thus creating higher-affinity sites for the protein without direct protein−base contacts. This has been suggested to explain the propensity for GC-rich sequences in some PKR binding sites (*29*). Given the fact that there are a small number of protein−base contacts in the Xlrbpa dsRBMII−RNA structure, these interactions may also contribute to selective binding (*18*). It is interesting to note that each of the RNAs investigated in this work has GC-rich sequence at the base of the stem−loop region. With the orientation of dsRBMI defined by our affinity cleavage experiments, we now know that loop 2 of dsRBMI is proximal to this region of the RNA. In the Xlrbpa crystal structure, loop 2 of the dsRBM is the only region of the protein that makes a base-specific contact with the duplex. This contact is between a backbone carbonyl oxygen and the 2-amino group of a guanosine in the minor groove. It is possible that amino acids found in the PKR dsRBMI loop 2 make specific base contacts in this GC-rich region, resulting in the observed binding selectivity. Affinity cleavage studies similar to those described here with stem−loop RNAs of varying sequence will be useful in testing this hypothesis. Defining the selectivity of PKR's RNA binding domain contributes to our understanding of RNA regulation of the kinase as this selectivity may dictate how PKR is organized on an RNA ligand and whether the RNA functions as a kinase activator or inhibitor.

The successful application of the affinity cleavage technique to localizing dsRBMI of PKR on stem−loop RNAs and defining its orientation suggest this approach could be applied to PKR's dsRBMII and dsRBMs found in other proteins. The dsRBMII of PKR contributes to the RNA binding affinity of the enzyme. Mutations in the conserved RNA binding residues of dsRBMII decrease the affinity of PKR's RBD for RNA, albeit to a lesser extent than mutations in dsRBMI (*25*). By modifying dsRBMII with EDTA·Fe, one could define its binding site and orientation on RNA ligands and determine to what extent the binding sites for dsRBMI and dsRBMII overlap and whether this varies for

different RNA ligands. These results would extend our understanding of PKR's RNA binding properties as well as delineate differences between PKR ligands that activate the kinase and those that inhibit the kinase. In addition, affinity cleavage using other dsRBM proteins modified with EDTA·Fe at positions analogous to E29 and D38 of PKR will allow the orientation of the modified dsRBM to be defined on the RNA. This could be particularly useful in understanding the specificity observed for these proteins, such as the sequence selectivity observed for substrates of the yeast RNaseIII homologue Rnt1p (*15*) or the editing selectivity observed for the RNA-editing adenosine deaminases ADAR1 and ADAR2 (*14*).

In summary, several significant conclusions can be made from this work. (a) The localized cleavage observed with PKR RBD EDTA·Fe conjugates indicates that the RNAs that have been studied have a limited number of binding sites for the protein. (b) dsRBMI of PKR's RBD binds these RNAs in a specific orientation, placing loop 2 at the base of the single-stranded loop and α1 near the duplex stem. (c) Deformations in the duplex of the synthetic stem−loop RNA, such as the base mismatches and nucleotide bulge, do not dictate the PKR dsRBMI binding preference. (d) The affinity cleavage technique has been shown to be applicable to the study of RNA binding by PKR and, by extension, other members of the dsRBM family of proteins.

ACKNOWLEDGMENT

We thank Prof. Claude Meares at the University of California, Davis, for the kind gift of bromoacetamidobenzyl-EDTA·Fe and suggestions for the modification chemistry. We also thank Mr. Nikolas Chmiel for helpful discussions and assistance with molecular modeling using the InsightII software package.

REFERENCES

1. Meurs, E., Chong, K., Galabru, J., Thomas, N. S. B., Kerr, I. M., Williams, B. R. G., and Hovanessian, A. G. (1990) *Cell 62*, 379−390.
2. Manche, L., Green, S. R., Schmedt, C., and Mathews, M. B. (1992) *Mol. Cell. Biol. 12*, 5238−5248.
3. Circle, D. A., Neel, O. D., Robertson, H. D., Clarke, P. A., and Mathews, M. B. (1997) *RNA 3*, 438−448.
4. Williams, B. R. G. (1999) *Oncogene 18*, 6112−6120.
5. DeHaro, C., Mendez, R., and Santoyo, J. (1996) *FASEB J. 10*, 1378−1387.
6. Kitajewski, J., Schneider, R. J., Safer, B., Munemitsu, S. M., Samuel, C. E., Thimmappaya, B., and Shenk, T. (1986) *Cell 45*, 195−200.
7. Clarke, P. A., Sharp, N. A., and Clemens, M. J. (1990) *Eur. J. Biochem. 193*, 635−641.
8. Fierro-Monti, I., and Mathews, M. B. (2000) *Trends Biochem. Sci. 25*, 241−246.
9. Bass, B. L., Nishikura, K., Keller, W., Seeburg, P. H., Emeson, R. B., O'Connell, M. A., Samuel, C. E., and Herbert, A. (1997) *RNA 3*, 947−949.
10. Bycroft, M., Gruenert, S., Murzin, A. G., and Proctor, M. (1995) *EMBO J. 14*, 3563−3571.
11. Kharrat, A., Macias, M. J., Gibson, T. J., and Nilges, M. (1995) *EMBO J. 14*, 3572−3584.
12. Langland, J. O., Kao, P. N., and Jacobs, B. L. (1999) *Biochemistry 38*, 6361−6368.
13. Jaramillo, M. L., Abraham, N., and Bell, J. C. (1995) *Cancer Invest. 13*, 327−338.
14. Melcher, T., Maas, S., Herb, A., Sprengel, R., Seeburg, P. H., and Higuchi, M. (1996) *Nature 379*, 460−464.
15. Nagel, R., and Ares, M. J. (2000) *RNA 6*, 1142−1156.
16. Schuldt, A. J., Adams, J. H. J., Davidson, C. M., Micklem, D. R., Haseloff, J., St. Johnston, D., and Brand, A. H. (1998) *Genes Dev. 12*, 1847−1857.
17. Nanduri, S., Carprick, B. W., Yang, Y., Williams, B. R. G., and Qin, J. (1998) *EMBO J. 17*, 5458−5465.
18. Ryter, J. M., and Schultz, S. C. (1998) *EMBO J. 17*, 7505−7513.
19. Ramos, A., Grunert, S., Adams, J., Micklem, D. R., Proctor, M. R., Freund, S., Bycroft, M., St. Johnston, D., and Varani, G. (2000) *EMBO J. 19*, 997−1009.
20. Bevilacqua, P. C., and Cech, T. R. (1996) *Biochemistry 35*, 9983−9994.
21. Spanggord, R. J., and Beal, P. A. (2000) *Nucleic Acids Res. 28*, 1899−1905.
22. Bevilacqua, P. C., George, C. X., Samuel, C. E., and Cech, T. R. (1998) *Biochemistry 37*, 6303−6316.
23. Akujarvi, G., Mathews, M. B., Anderson, P., Vennstrom, B., and Pettersson, U. (1980) *Proc. Natl. Acad. Sci. U.S.A. 77*, 2424−2428.
24. Schultz, P. G., Taylor, J. S., and Dervan, P. B. (1982) *J. Am. Chem. Soc. 104*, 6861−6863.
25. Green, S. R., Manche, L., and Mathews, M. B. (1995) *Mol. Cell. Biol. 15*, 358−364.
26. DeRiemer, L. H., Meares, C. F., Goodwin, D. A., and Diamanti, C. I. (1981) *J. Labelled Compd. Radiopharm. 18*, 1517−1534.
27. Joseph, S., Whirl, M. L., Kondo, D., Noller, H. F., and Altman, R. B. (2000) *RNA 6*, 220−232.
28. Clemens, M. J., Laing, K. G., Jeffrey, I. W., and Schofield, A. (1994) *Biochimie 76*, 770−778.
29. Clarke, P. A., and Mathews, M. B. (1995) *RNA 1*, 7−20.
30. Pendergrast, P. S., Ebright, Y. W., and Ebright, R. H. (1994) *Science 265*, 959−962.
31. Oakley, M. G., and Dervan, P. B. (1990) *Science 248*, 847−850.
32. Heilek, G. M., and Noller, H. F. (1996) *Science 272*, 1659−1662.
33. Lehmann, K. A., and Bass, B. L. (1999) *J. Mol. Biol. 291*, 1−13.

BI002512W